Contaminant source and aquifer characterization using geophysical data and the Ensemble Smoother with Multiple Data Assimilation

Zi Chen[a,b], Leli Zong[a], J. Jaime Gómez-Hernández[d], Teng Xu[c,*], Yuehua Jiang[a,b], Quanping Zhou[a,b], Hai Yang[a,b], Zhengyang Jia[a,b], Shijia Mei[a,b]

[a] *Nanjing Center, China Geological Survey, Nanjing, China*
[b] *Key Laboratory of Watershed Eco-Geological Processes, Ministry of Natural Resources, Nanjing, China*
[c] *State Key Laboratory of Hydrology-Water Resources and Hydraulic Engineering, Hohai University, Nanjing, China*
[d] *Institute of Water and Environmental Engineering, Universitat Politècnica de València, Valencia, Spain*

Abstract

Contaminant source and aquifer characterization (CSAC) is critical in groundwater pollution evaluation and remediation. The ensemble smoother with multiple data assimilation (ES-MDA) is employed to jointly identify contaminant source information and hydraulic conductivities by assimilating time-lapse electrical resistivity tomography (ERT) data. In a synthetic profile with a time-varying release history in a heterogenous aquifer, we verify the performance of the proposed data assimilation framework. The results show that the CSAC problem could be handled by the proposed approach. The time-varying release history and the high permeability area can be identified with adequate time-lapse ERT measurements. Further reproduction of the evolution of the plume after CSAC also shows consistency with the reference plume. Data redundancy caused by the correlation between the measurements is also analyzed through the comparison of four scenarios with different apparent resistivity measurements. In the scenario with an AM-BN scheme with three different electrode spacing, the identification result suffers from data redundancy and ends up with a poor inversion. Properly accounting for correlated measurements, the proposed ES-MDA data assimilation

*Corresponding author
Email address: teng.xu@hhu.edu.cn (Teng Xu)

framework could provide convincing inversion of time-varying releasing history and hydraulic conductivities.
Keywords: Coupled modeling, Release history, Hydraulic conductivity, Data assimilation, Inversion

1. Introduction

Aquifers are a fundamental component of the hydrologic cycle, crucial for water supply and with many dependent ecosystems. Unfortunately, they can be easily polluted by anthropogenic activities, such as landfill operations, industry leakages, urban sewages, and others. Groundwater contamination is an important issue that has drawn the attention of researchers in the past decades (Gómez-Hernández and Wen, 1994; Gómez-Hernández et al., 2003; Feyen et al., 2003; Li et al., 2011; Megdal, 2018). A critical issue in groundwater contamination is the identification of the source of contamination together with the characterization of aquifer properties, mainly hydraulic conductivity. Inverse problems in hydrogeology have been the focus of many researchers, who have found that it is an ill-posed problem of difficult solution (Carrera and Neuman, 1986; Capilla et al., 1998, 1999; Wen et al., 1999; Franssen and Gómez-Hernández, 2002; Bagtzoglou and Atmadja, 2005; Jiang et al., 2021). Joint inversion of

To date, several methods have been developed for contaminant source identification and there are several good reviews available (Atmadja and Bagtzoglou, 2001; Michalak and Kitanidis, 2004; Gómez-Hernández and Xu, 2021). The proposed methods could be grouped into three main categories: optimization, probabilistic, and backward-in-time simulation methods. The optimization approaches build an objective function and attempt to minimize the discrepancies between simulated and observed measurements (Gorelick et al., 1983; Sun et al., 2006; Mirghani et al., 2009; Ayvaz, 2010; Li et al., 2012); the probabilistic approaches handle the problem in a stochastic framework and try to maximize the posterior probabilities of the simulated measurements conditioned on the observed ones (Woodbury and Ulrych, 1996; Zeng et al., 2012; Butera et al., 2013; Cupola et al., 2015; Pirot et al., 2019); backward-in-time simulation methods solve the solute transport equations backward to identify the most likely contaminant release locations (Bagtzoglou et al., 1992; Neupauer and Wilson, 1999; Bagtzoglou and Atmadja, 2003; Ababou et al., 2010).

In recent years, data assimilation methods have become increasingly prominent for their versatile and efficient features. The ensemble Kalman filter (EnKF) proposed by Evensen (2003) and the ensemble smoother with multiple data assimilation (ES-MDA) proposed by Emerick and Reynolds (2013) have been progressively employed for contaminant source identification. Xu and Gómez-Hernández (2016) first proposed the restart normal-score EnKF to solve the contaminant source identification problem and then extended this method for the simultaneous identification of both contaminant source and aquifer heterogeneous conductivity (Xu and Jaime, 2018). Li et al. (2019) combined a mixed integer nonlinear programming optimization model with a Kalman filter to deduce contaminant source information. Panjehfouladgaran and Rajabi (2022) combined artificial neural networks and constrained the restart EnKF to characterize the contaminant source in a coastal aquifer and then moved one step further to identify aquifer heterogeneity in a tide-influenced coastal aquifer (Dodangeh et al., 2022). The ES-MDA method has been coupled with generative adversarial networks by Bao et al. (2020) to handle a channelized aquifer characterization problem. Todaro et al. (2021) applied the ES-MDA method to identify contaminant source location and release history. Xu et al. (2022) addressed the problem of non-point source identification via ES-MDA.

The aforementioned research findings are proof of the capacity of data assimilation methods for the joint identification of contaminant sources and aquifer heterogeneity, however, despite a few applications in sandbox experiments, there is still a lack of verification in field cases. One main reason is that the measurements required are not available; at most, only a few sparse and discontinuous pollution data are accessible. One possible solution to the lack of contaminant data could be the use of geophysical surveys. Geophysical methods have been broadly utilized in groundwater contamination investigation, especially electrical resistivity tomography (ERT), which is a non-intrusive, cost-effective, and high sampling density method (Seferou et al., 2013; Binley et al., 2015; Mao et al., 2016; Shao et al., 2021; Xia et al., 2021). ERT could be the perfect data source for ensemble-based contaminant source identification problems. As far as we know, several works have already combined data assimilation methods with ERT to study groundwater contamination issues. Bouzaglou et al. (2018) combined the EnKF method and the SUTRA model to update groundwater states and soil parameters by using ERT measurements in a seawater intrusion laboratory experiment. Kang et al. (2018) first developed an EnKF-based data assimilation algorithm to jointly invert DNAPL saturation and a hydraulic conductivity field by using time-lapse ERT data and later employed the ensemble smoother-direct sampling method (ES-DS) to identify a non-Gaussian hydraulic conductivity field by assimilating both geochemical and time-lapse geophysical datasets (Kang et al., 2019). Tso et al. (2020) proposed an ensemble-based data assimilation framework to jointly identify contaminant source location, initial release time, and solute loading from cross-borehole time-lapse ERT data. None of these works jointly addresses contaminant source identification and aquifer characterization.

In this paper, we propose the ensemble smoother with multiple data assimilations (ES-MDA) to identify jointly contaminant source and aquifer heterogeneity by using time-lapse ERT data. Different cross-hole configurations are explored. To the best of our knowledge, it is the first time that the ES-MDA is used to jointly identify a contaminant source and aquifer heterogeneity. The paper is organized as follows: First, in section 2, we introduce the methodology of the proposed data assimilation framework, including the coupling of groundwater flow, solute transport, and geophysical modeling into the ES-MDA implementation; then, in sections 3, a synthetic case with a time-varying releasing history in a heterogenous aquifer property is built that will be used as the reference to test the proposed method; section 4 evaluates and discusses the proposed approach, and the paper ends with a summary and conclusions of the main findings in section 5.

2. Methodology

2.1. Groundwater flow and solute transport model

Transient groundwater flow and solute transport in an aquifer can be described by the following partial differential equations (Bear, 1972; Zheng and Wang, 1999)

$$S_s \frac{\partial h}{\partial t} = \nabla \cdot (K \nabla h) + w, \tag{1}$$

$$\frac{\partial (\theta C)}{\partial t} = \nabla \cdot (\theta D \cdot \nabla C) - \nabla \cdot (\theta v C) - q_s C_s, \tag{2}$$

where S_s represents specific storage $[L^{-1}]$; h stands for hydraulic head $[L]$; t denotes time $[T]$; $\nabla \cdot$ and ∇ are the divergence and gradient operators, respectively; K represents hydraulic conductivity $[LT^{-1}]$; w represents distributed sources or sinks $[T^{-1}]$, θ represents porosity of the medium [-]; C is dissolved concentration $[ML^{-3}]$; D is a hydrodynamic dispersion coefficient tensor $[L^2T^{-1}]$; v stands for the flow velocity vector $[LT^{-1}]$ derived from the solution of Eq. (1); q_s represents volumetric flow rate per unit volume of aquifer associated with a fluid source or sink $[T^{-1}]$ and C_s is concentration of the source or sink $[ML^{-3}]$. The solution of both equations requires the specification of initial and boundary conditions. In this work, the flow equation is numerically solved using the finite difference MODFLOW program Harbaugh (2005) and the transport equation using the finite difference MT3D program Bedekar et al. (2016).

2.2. Geophysical model

The electrical potential field induced by a couple of electrodes can be described by the following equation

$$-\nabla \cdot \frac{1}{\rho}\nabla V = I(\delta(\mathbf{r}-\mathbf{r}_+) - \delta(\mathbf{r}-\mathbf{r}_-)), \tag{3}$$

where ρ is porous media resistivity; V denotes electrical potential field; I is the input current from a dipole; $\mathbf{r}_+$ and $\mathbf{r}_-$ are the locations of the positive and negative electrodes, respectively, and $\delta(\cdot)$ is the Dirac delta function.

The electrical resistivity of the porous medium depends on several factors, such as porosity or pore water conductivity. The resistivity model developed by Revil et al. (2018) is employed in this work

$$\frac{1}{\rho} = (S_w\phi)^m\sigma_w + (S_w\phi)^{m-1}\rho_s(B-\lambda)CEC, \tag{4}$$

where S_w is water saturation, which equals 1 in aquifers; ϕ is porosity, which in this study is 0.32 for both the coarse and fine sands (Power et al., 2013); m is a cementation exponent; ρ_s is grain density; B and λ are apparent mobility of the counterions responsible for surface conduction and polarization, respectively; CEC is the quantity of exchangeable cation on the surface of the mineral; and σ_w is pore water conductivity, which is related to the ionic concentration and temperature (Sen, 1992) according to the following expression

$$\sigma_w = (5.6 + 0.27T - 1.5\times 10^{-4}T^2)C - (\frac{2.36+0.099T}{1.0+0.214C})C^{\frac{2}{3}}, \tag{5}$$

where T is temperature, which is assumed constant at 25 °C in this research; and C is ionic concentration.

Apparent resistivities (ρ_a), which are the values observed in an ERT survey, are computed from the resistivity values obtained from Eq. (4) solving a geophysical forward problem using the finite-element open-source software ResIPy (Blanchy et al., 2020).

The combination of MODFLOW, MT3D, Eq. (4) and (5) and ResIPy serve to establish the relationship between apparent resistivity ρ_a and concentration C.

2.3. Ensemble Smoother with Multiple Data Assimilation (ES-MDA)

The ES-MDA technology is employed to identify a contaminant source and aquifer heterogeneity from apparent resistivity data. A short description of the ES-MDA is provided next, for a more in-depth discussion the reader is referred to Emerick and Reynolds (2013):

1. Procedure

The first step of the ES-MDA technology is to generate N_e realizations with unknown CSAC parameters, which include time-varying release history and hydraulic conductivity spatial distribution in this work. Once the number of iterations N_a and the inflation factor α_j (explained in detail below) are determined, the method will go through two steps: forecast step and analysis step.

In the forecast step, the groundwater flow, solute transport and geophysical models (MODFLOW, MT3DS and ResIPy), are run for each member of the ensemble,

$$B_{i,j}^f = \psi[B_0, A_{i,j}], \tag{6}$$

for $i = 1, 2, \ldots, N_e$, and $j = 1, 2, \ldots, N_a$, where B^f stands for the vector of forecasted apparent resistivity, and B_0 for the vector of initial apparent resistivities; ψ represents the forward numerical model; A is the vector of CSAC parameters, including source release history and hydraulic conductivity distribution.

Then, the CSAC parameters are updated using a truncated singular value decomposition (TSVD) method in the analysis step,

$$A_{i,j+1} = A_{i,j} + \Delta A_j (\Delta B_j^f)^T [\Delta B_j^f (\Delta B_j^f)^T + \alpha_j R]^{-1} [y_{obs} + \sqrt{\alpha_j}\varepsilon - B_{o,i,j}^f], \tag{7}$$

where y_{obs} is a column vector with dimensions $N_o \cdot N_t$ of real measurements (N_o stands for the number of apparent resistivity measurements, and N_t the number of observation time steps); ε stands for the observation error, while R is the covariance matrix of the observation error; $B^f_{o,i,j}$ stands for the vector of forecasted apparent resistivity at observation locations; ΔA_j and ΔB_j are square root matrices defined as

$$\Delta A_j = \frac{1}{\sqrt{N_e - 1}}[A_{1,j} - \overline{A}_j, A_{2,j} - \overline{A}_j, \ldots, A_{N_e,j} - \overline{A}_j], \tag{8}$$

$$\Delta B^f_j = \frac{1}{\sqrt{N_e - 1}}[B^f_{1,j} - \overline{B^f}_j, B^f_{2,j} - \overline{B^f}_j, \ldots, B^f_{N_e,j} - \overline{B^f}_j], \tag{9}$$

where $\overline{A}_j$ and $\overline{B^f}_j$ are the ensemble means of the CSAC parameters subject to identification and of the forecasted apparent resistivity at the j_{th} iteration, respectively.

2. Inflation factor

The inflation factor α_j is influential to the performance of the ES-MDA, and several ways on how to compute them have been described in previous studies (Le et al., 2016; Rafiee and Reynolds, 2017; Evensen, 2018). In this work, based on our previous experience ADD REFERENCE HERE, to the JCH paper or your PhD thesis , we decide to apply the inflation factor scheme proposed by Rafiee and Reynolds (2017).

The inflation factor at the first assimilation step is given by

$$\alpha_1 = (\frac{1}{N}\sum_{i=1}^{N}\lambda_i)^2, \tag{10}$$

where N is the minimum of N_e and $N_o \cdot N_t$; and λ_i are the singular values of the matrix D_j given by

$$D_j = R^{-\frac{1}{2}} \triangle B^f_j. \tag{11}$$

The subsequent inflation factors are chosen in a geometrical decreasing progression,

$$\alpha_j = \beta^{j-1}\alpha_1, \tag{12}$$

where β is the ratio that ensures that the sum of the inverse of the inflation factors equals one. Its value is given by

$$\frac{1-(1/\beta)^{N_a-1}}{1-1/\beta} = \alpha_1. \tag{13}$$

3. The normal-score transformation

Although ES-MDA is capable of dealing with non-linear models, it failed when the augmented state followed a non-Gaussian distribution (Zhou et al., 2014; Cao et al., 2018). To address this problem, several methods have been proposed, such as using Gaussian mixture models, iterative approaches, reparameterizations, and normal-score transform (Hendricks Franssen and Kinzelbach, 2008; Zhou et al., 2011; Kumar and Srinivasan, 2019). In this paper, the normal-score transform algorithm is combined with ES-MDA to deal with non-Gaussianity. The main procedure of this method follows two steps: (i) transform the non-Gaussian augmented state vector into a marginally-Gaussian vector, and then perform ES-MDA in Gaussian space; (ii) back transform the ES-MDA updates into original space. Although the normal-score transform algorithm does not ensure that higher-order moments will follow a multi-Gaussian distribution (Jafarpour and Khodabakhshi, 2011; Kumar and Srinivasan, 2020), the outcome of normal-score ES-MDA outperforms ES-MDA for clearly non-Gaussian parameters.

2.4. Data assimilation workflow

Figure 1 shows the overall description of the proposed data assimilation workflow. Using this workflow, we are able to jointly update the non-Gaussian hydraulic conductivity and source release history by assimilating the apparent resistivity. Note that since MODFLOW

Framework: ES-MDA with coupled models
• Generate initial ensemble, A_0 (including K_0,C_0).
• Choose the number of ES-MDA iterations, N_a.
• For $j = 1\ to\ N_a$
◦ Set $A^f_{i,j} = A^a_{i,j-1}$ for $i = 1, 2, ...N_e$.
◦ Run the groundwater flow and solute transport model in each realization.
◦ Calculate ρ using (4) and (5).
◦ Run the geophysical model, obtain apparent resistivity ρ_a.
◦ Calculate α_j using (10),(11),(12) and (13).
◦ Apply the normal-score transformation.
◦ Update model parameters $A^a_{i,j}$ based on (7).
◦ Apply the normal-score back transformation.
• Endfor

Figure 1: Overall description of the proposed data assimilation framework.

and MT3DS are finite-difference numerical methods, while ResIPy is a finite-element method, an extra grid refinement procedure is needed before the geophysical model is run.

3. Application

3.1. Synthetic profile description

To test the proposed data assimilation framework, a non-Gaussian confined aquifer with a time-varying contaminant release is constructed. The contaminant moves in a two-dimensional synthetic sandbox of $40 \times 1 \times 20$ m, time-lapse ERT is simulated to capture the evolution in time of the pollutant concentration.

The profile model is discretized into 80 by 1 by 40 cells, each cell being 0.5 by 1 by 0.5 m. The synthetic sandbox is filled with fine and coarse sand, according to a spatial arrangement generated using a truncated Gaussian simulation (Journel and Isaaks, 1984) with the first quartile as the truncation threshold, resulting in a coarse sand proportion of 0.25, as shown in Figure 2 MISSING INFORMATION: how the coarse sand conductivity values are generated. Later, in the table, the coarse sand is listed as homogeneous, in which case, the realization in Fig. 1 should be replaced, as is, it shows heterogeneity . The boundary conditions are set as follows: the upper and lower boundaries are impermeable; the left boundary is a constant head boundary of $30m$; the right boundary is zero-flow, except for the top four cells that are time-varying income flow through which the contaminant enters the sandbox. Such contamination could mimic the release from a contaminated river or irrigation canal in reality. The release pattern follows the same bimodal pulse proposed by Skaggs and Kabala (1994) and used many times later by others (Figure 2) given by:

$$C(t) = 2 \cdot \exp(-\frac{(t-10)^2}{35}) + 0.6 \cdot \exp(-\frac{(t-25)^2}{80}) + \exp(-\frac{(t-45)^2}{40}) \qquad 0 \leq t \leq 100 \tag{14}$$

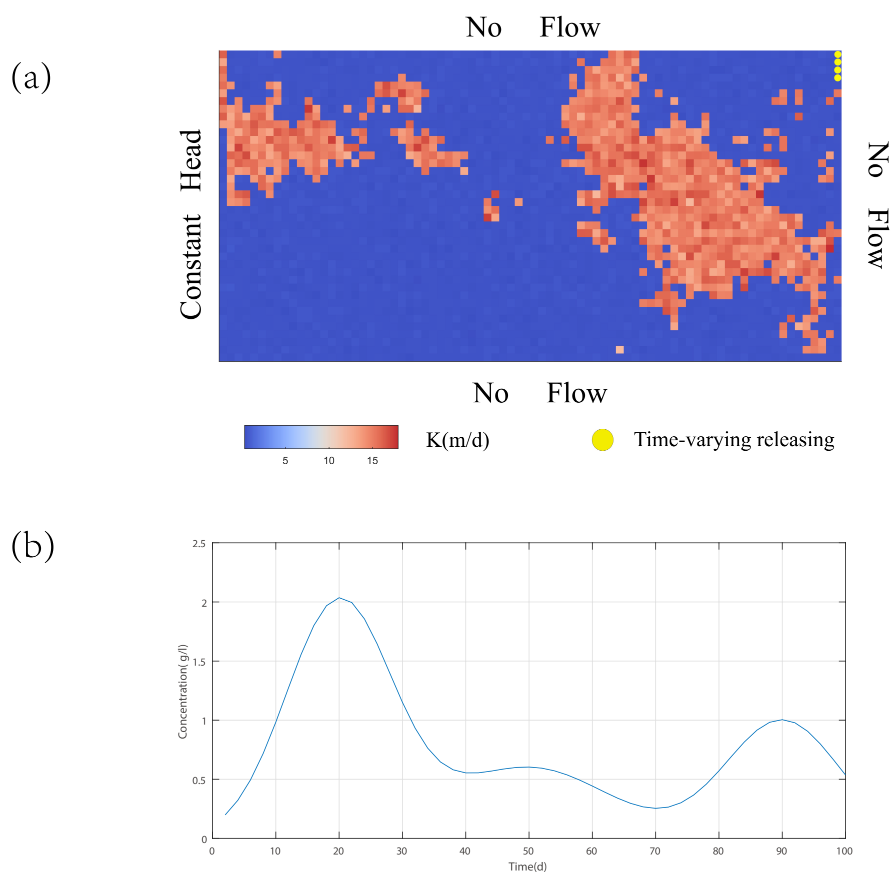

Figure 2: Schematic view of the groundwater flow and solute transport reference model. (a) Flow boundary conditions and reference hydraulic conductivity field. (b) Reference concentration release curve.

For the time-lapse ERT, 30 electrodes are assigned in three vertical boreholes with an

Table 1: Definition of the synthetic scenarios

	Scenario 1	Scenario 2	Scenario 3	Scenario 4
Vertical separation distance, a (m)	6	4	2	2, 4 and 6
Number of ρ_a measurements	98	128	162	388

interval of 2 m as shown in Figure 3. A and B represent the current electrodes, while M and N represent the potential electrodes. We adopt the bipole-bipole electrode array configuration based on previous research since the cross-hole AM-BN configuration yields greater flexibility in practice without any singularity problem in data acquisition (Zhou and Greenhalgh, 2000). In this paper, the separation between the electrodes BN is kept the same as those in AM (AM=BN=a). Three vertical separation distance values are analyzed (a=6 m, 4 m, 2 m). Four different numbers of ρ_a measurements are considered (98, 128, 162, and 388). See Table 1 for the list of scenarios analyzed. In scenario S1, a sparse AM-BN scheme with an electrode spacing of 6 m is used (98 measurements per time step, 980 in total). This is a relatively small amount of measurements in a time-lapse ERT survey but could happen in reality when limited data processing capabilities are available (Binley and Kemna, 2005). We gradually increase the number of measurements in scenarios S2 and S3, with AM-BN schemes of 128 and 162 measurements, respectively. In scenario S4, all three electrode separation distances are used, resulting in a total of 388 measurements per time step. WARNING. The description of the ERT measurement is not very clear. The arrow with the "2m" label in figure 3b does not help to understand anything

You must show also the reference hydraulic heads, a couple of snapshots of the reference concentration, AND the reference resistivity for those snapshots

The total simulation time of groundwater flow and transport solute is 100 days, and the models are run in 50 equal-sized time steps. As for the geophysical model, the measurements are acquired with a time interval of 10 days. A more detailed description of the parameters used in the MODFLOW, MT3DS and ResIPy models are listed in Table 2.

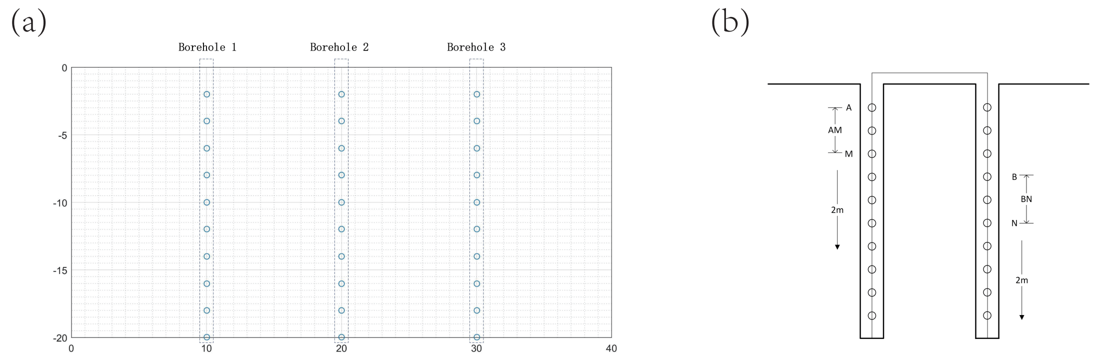

Figure 3: Schematic view of the geophysical synthetic model. (a) The distribution of the boreholes and electrodes. The black dotted box represents the borehole; the blue circle stands for a single electrode. (b) Configuration of the bipole-bipole electrodes array. A and B represent the current electrodes, M and N represent the potential electrodes. THIS FIGURE IS HARD TO READ. You may wish to put (a) on top of (b) instead of side by side

For the assimilation phase, and based on our previous work (Chen et al., 2018, 2021; Xu et al., 2021), the number of iterations (N_a) is chosen to be 4, the ensemble size (N_e) is taken as 500. The initial hydraulic conductivity distribution fields are generated from the same algorithm as the reference one, while the initial release history is generated as constant in time using a uniform distribution with ranges [0.5, 1.5] g/l. The model error is neglected and the ρ_a measurements errors follow Gaussian distribution with a mean of 0 and standard deviation of 0.1 $\Omega \cdot m$, which amounts to approximately 2.68% relative error.

3.2. Performance Assessment

The use of an ensemble-based method allows to analyze the performance of the method using the root mean square error (RMSE) and the relative RMSE:

$$RMSE = \sqrt{\frac{1}{n}\sum_{i=1}^{n}(A^{ref} - \overline{A}_i)^2}, \tag{15}$$

where n is the number of points used to discretize the release history curve or the number of cells in which hydraulic conductivity must be identified, A^{ref} is the reference CSAC parameters while $\overline{A}$ stands for the ensemble mean of the updated CSAC parameters. The

Table 2: Groundwater flow, solute transport, geophysical model parameters

Parameters	Value
Model discretization	
model length along x (m)	40
model length along y (m)	1
model height along z (m)	20
grid size $\Delta x \times \Delta y \times \Delta z$(m)	$0.5 \times 1 \times 0.5$
total simulation time (d)	100
time step length (d)	2
number of time steps	50
Groundwater flow model parameters	
hydraulic conductivity, coarse sand (m/d)	15
hydraulic conductivity, fine sand (m/d)	0.5
Solute transport model parameters	
longitudinal dispersivity (m)	0.5
transverse dispersivity (m)	0.025
molecular diffusion coefficient	0
initial water concentration (g/l)	0.15
Geophysical model parameters	
porosity, coarse sand & fine sand	0.32[a]
CEC, coarse sand & fine sand(C/kg)	7.2[a]
Cementation exponent, coarse sand & fine sand	2.0[a]
$B(\mathrm{m}^{-2}\mathrm{s}^{-1}\mathrm{V}^{-1})$	4.1×10^{-9} [b]
$\lambda(\mathrm{m}^{-2}\mathrm{s}^{-1}\mathrm{V}\text{-}1)$	3.46×10^{-10} [b]

[a] Power et al. (2013).
[b] Revil et al. (2018).

smaller the values for RMSE, the better the estimation of the CSAC parameters.

4. Results

4.1. Contaminant source and aquifer characterization

Figure 4 shows the recovered release histories for scenario S1 to S4. In each plot, the blue curve corresponds to the actual release history, the gray lines are the recovered release history curves for all 500 realizations, the red dotted lines are the median, and the black dashed lines are the 5 and 95 percentiles. It can be observed that the median of the recovered release history curves follows the true release in all scenarios, but with an excess of fluctuation. This noticeable fluctuation in the ensemble medians and individual curves is believed to be caused by the inherent ill-posedness of identification problem (**?**). For scenarios S1 to S3, the increase in the number of measurements seems to improve the overall uncertainty as given by the width of the 90% confidence interval. However, in Scenario S4, with the largest number of observations with an AM-BN scheme with 388 measurements, the 90% confidence interval gets too narrow and in several instants does not contain the reference release curve. The calculated $RMSE_c$ for all scenarios is shown in Table 3 and reinforces the previous statements. For scenarios S1 to S3, the $RMSE_c$ declines gradually with the increasing of measurements, while in scenario S4, the $RMSE_c$ has a value second only to the initial ensemble. We believe the poorly conditioned inversion in scenario S4 is mainly caused by data redundancy, which is quite common in reservoir modeling (Evensen and Eikrem, 2018). One more thing that needs to be pointed out is the bad estimation of the release curve for the last time steps. This outcome can be explained in that there are not enough data for the ES-MDA method to estimate the release at the latest release times.

As for aquifer characterization, Figure 5 shows the ensemble means and variances of hydraulic conductivities for the initial ensemble and scenarios S1 to S4. The ensemble mean of the hydraulic conductivities in the initial ensemble is relatively homogenous, while the

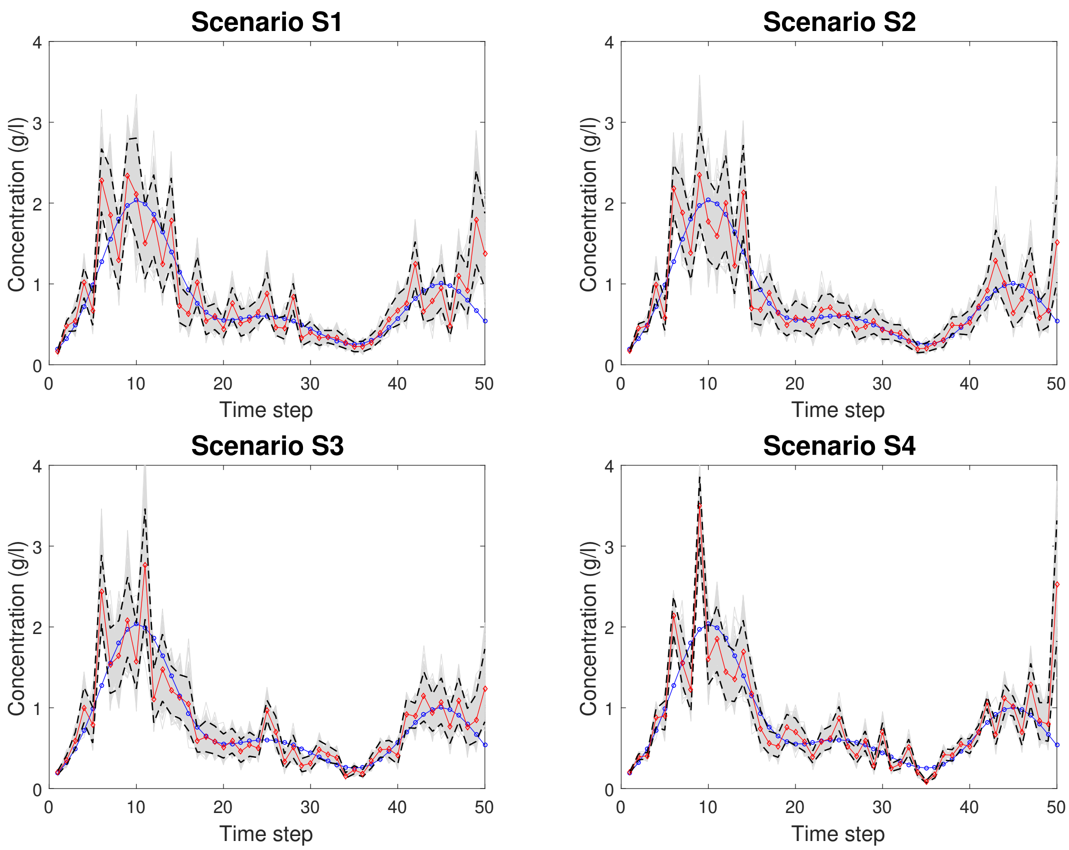

Figure 4: Recovered release histories for scenarios S1 to S4. The blue curve corresponds to the reference release history. The gray lines are the recovered release history curves for all 500 realizations, the red dotted lines are the median, and the black dashed lines are the 5 and 95 percentiles.

ensemble variance takes a large value. After assimilating the geophysical measurements, the ensemble mean of the updated hydraulic conductivities can delineate roughly the facies distribution in the aquifer with a substantial reduction of the ensemble variance in all scenarios. Further comparison between different scenarios shows that S3 has the best aquifer characterization, with a clear identification of the high permeability area and a relatively small ensemble variance, while S1 and S2 could delineate the high hydraulic conductivity zone less precisely and with a larger variance. In Scenario S4, a similar outcome to S3 is obtained, but with a poorer description of the high permeability area. A quantitative evaluation of all scenarios is listed in Table 3. Once again, we could find out that S4 has an $RMSE_K$ value much greater than S1 to S3, possibly due to data redundancy. This outcome is contrary to

Table 3: Performance of the scenario S1 to S4

	Initial ensemble	Scenario 1	Scenario 2	Scenario 3	Scenario 4
$RMSE_C$	0.535	0.331	0.289	0.287	0.423
$RMSE_K$	7.435	6.543	6.927	6.743	7.290

the general understanding (the more data the better the characterization), but is consistent with the findings by Evensen and Eikrem (2018) when the measurements have an inherent correlation. In this case, the AM-BN schemes with different electrodes spacing (2 m, 4 m, 6 m) typically have correlated measurement errors, so the mixture of three AM-BN schemes in S4 suffers from strong conditioning on the geophysical data and finally ends up with a poorly conditioned inversion.

4.2. Contaminant plume reproduction

For a further evaluation of the results, we use the updated CSAC to generate snapshots of the contaminant plume evolution to visually analyze the performance of the ES-DMA. Figure 6-9 show the reference plume, and the ensemble mean plumes computed with the initial set of CSAC parameters and with the updated CSAC values for all 4 scenarios in days 20, 40, 70 and 90. The ensemble mean plumes generated by the initial ensemble spread widely with very large uncertainty since no observed data have been assimilated yet. The comparison between the reference and simulated contaminant plumes speaks favorably about the proposed methodology since for all 4 scenarios main contaminant plume morphology is captured at the different time snapshots. A closer look, point to S3 as the scenario that performs best, especially in days 20 and 90.

Figures 10-12 show the time evolution of the vertically-averaged concentration along the boreholes 1, 2, and 3 for all 4 scenarios computed with the updated CSAC parameters. The blue curve corresponds to the evolution of the concentration in the reference, while the gray lines are the concentration curves for all 500 realizations, and the red line is the ensemble median. The shape of the concentration curves is well reproduced in all scenarios. Again, a closer look shows that scenario S3 performs best, especially in borehole 1.

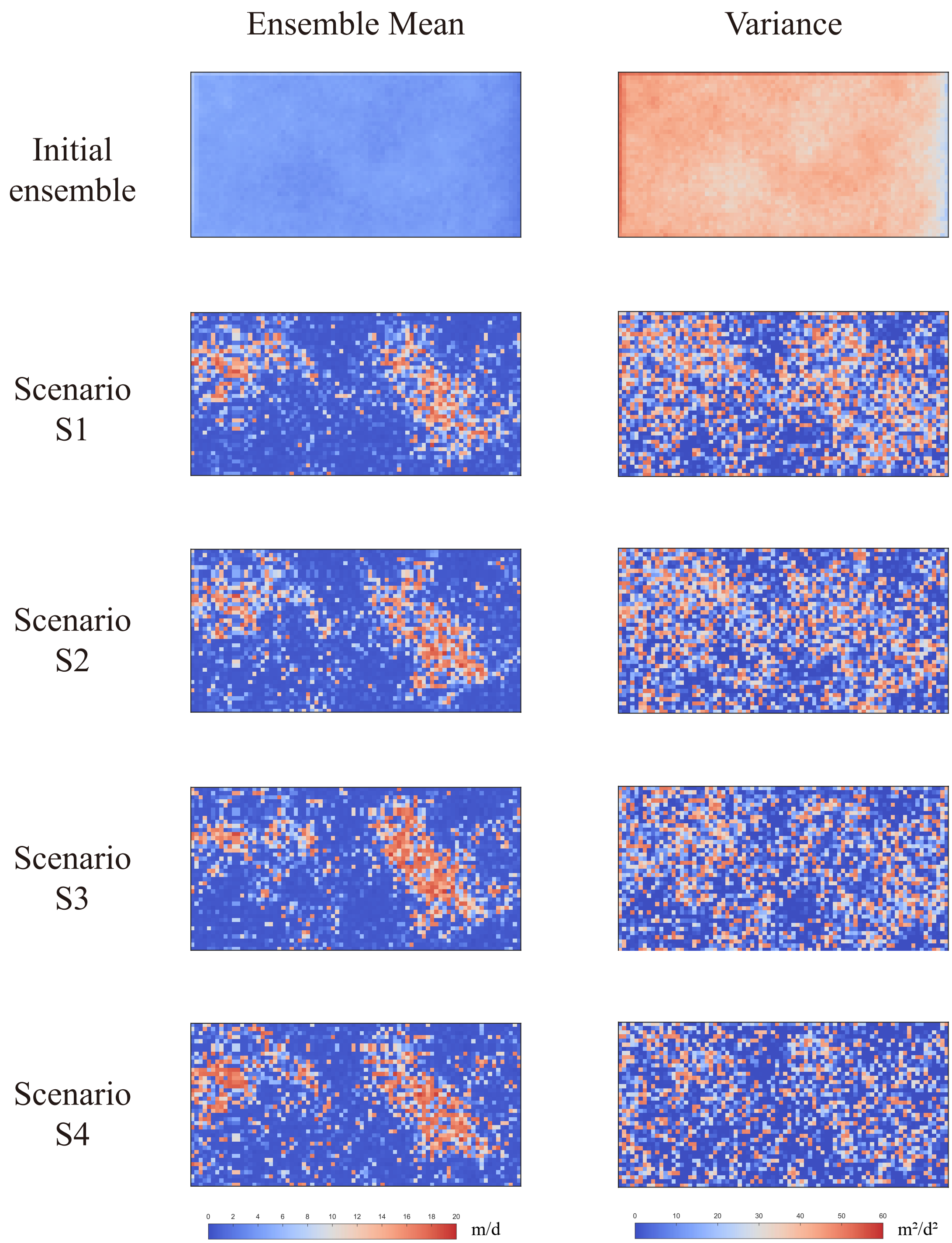

Figure 5: Ensemble means and variances of hydraulic conductivities for the initial ensemble and scenarios S1 to S4.

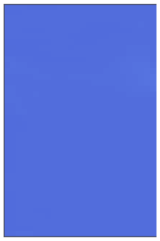

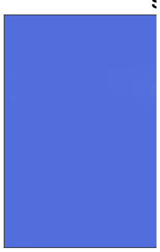

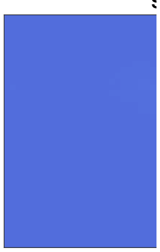

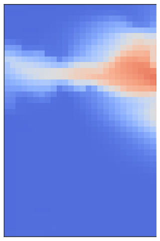

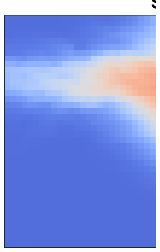

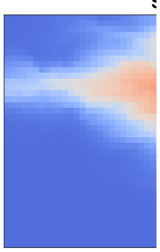

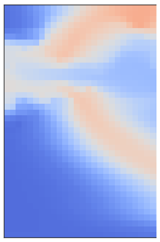

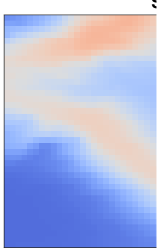

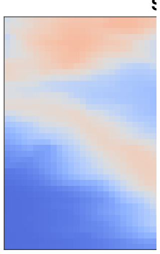

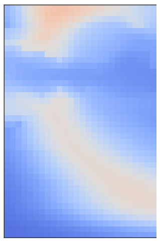

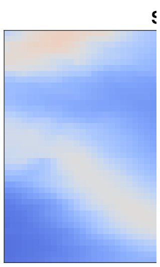

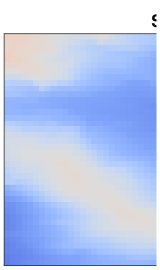

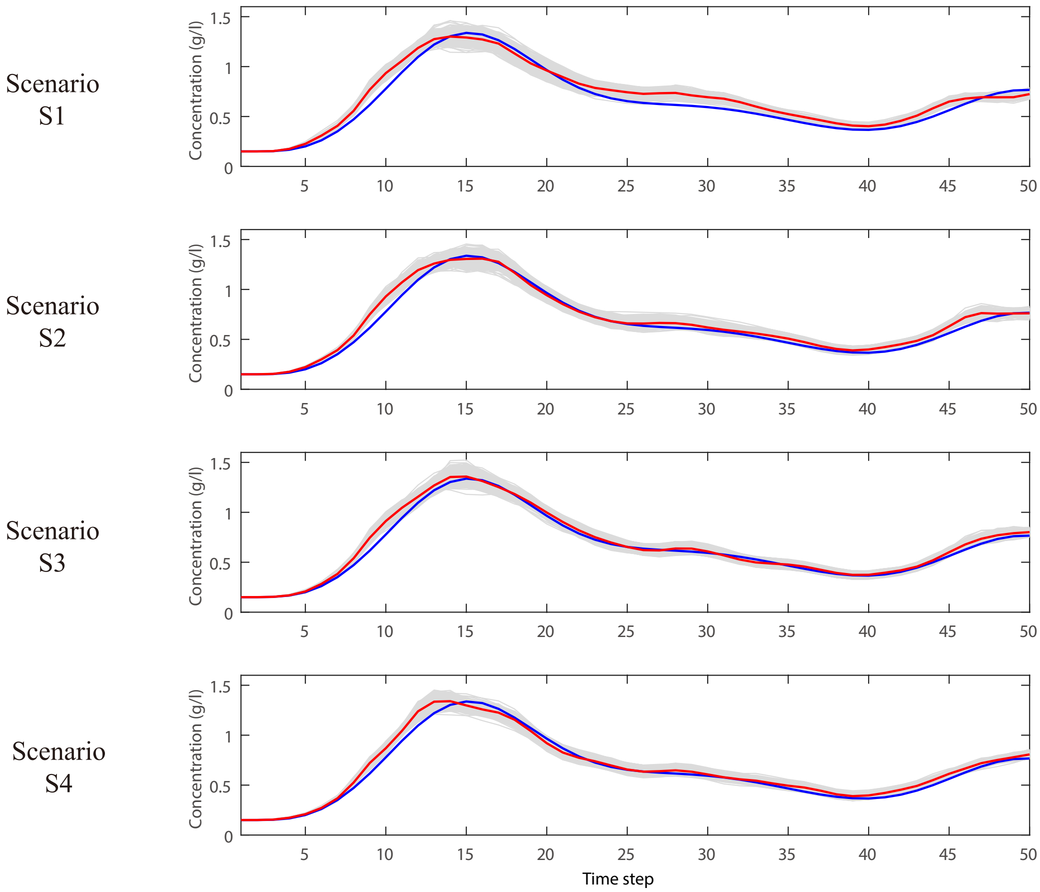

Figure 10: Time evolution of the vertically-averaged concentration of the recovered plume in borehole 1 for all 4 scenarios. The blue curve corresponds to the evolution of the concentration in the reference, while the gray lines are the concentration curves for all 500 realizations, and the red line is the ensemble median.

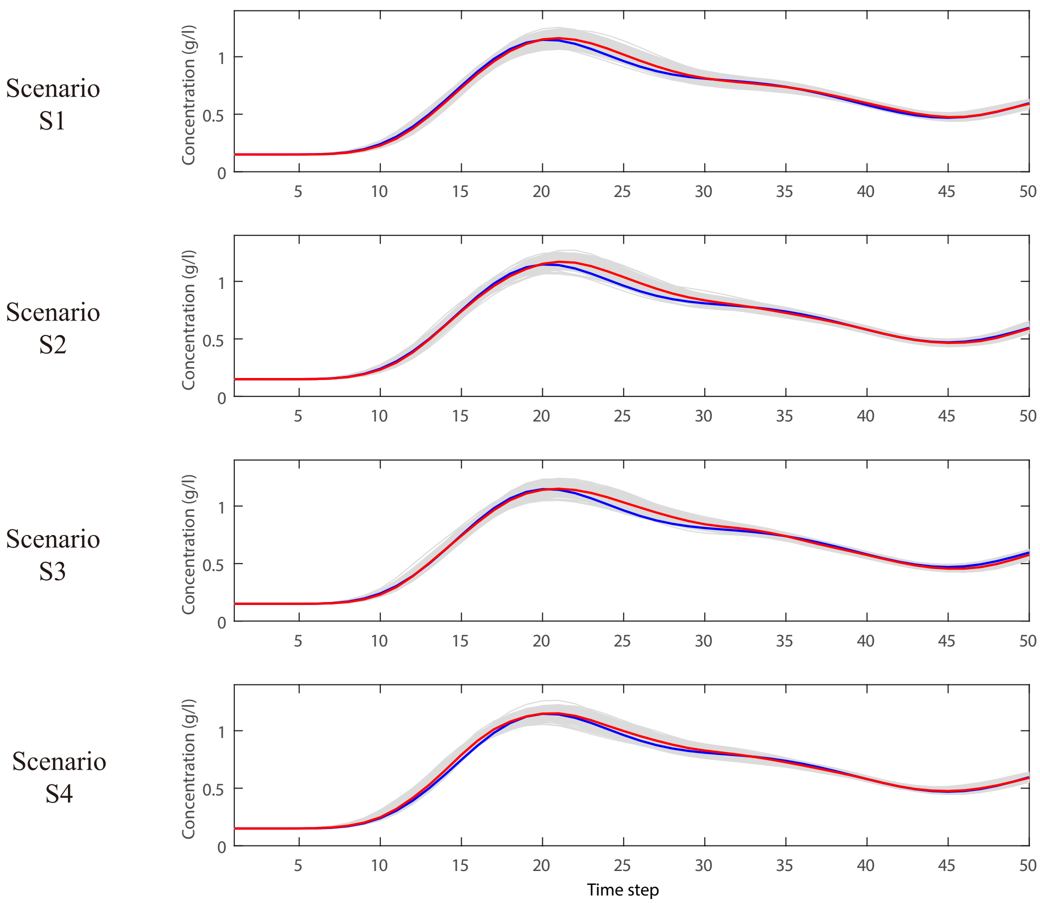

Figure 11: Time evolution of the vertically-averaged concentration of the recovered plume in borehole 2 for all 4 scenarios. The blue curve corresponds to the evolution of the concentration in the reference, while the gray lines are the concentration curves for all 500 realizations, and the red line is the ensemble median.

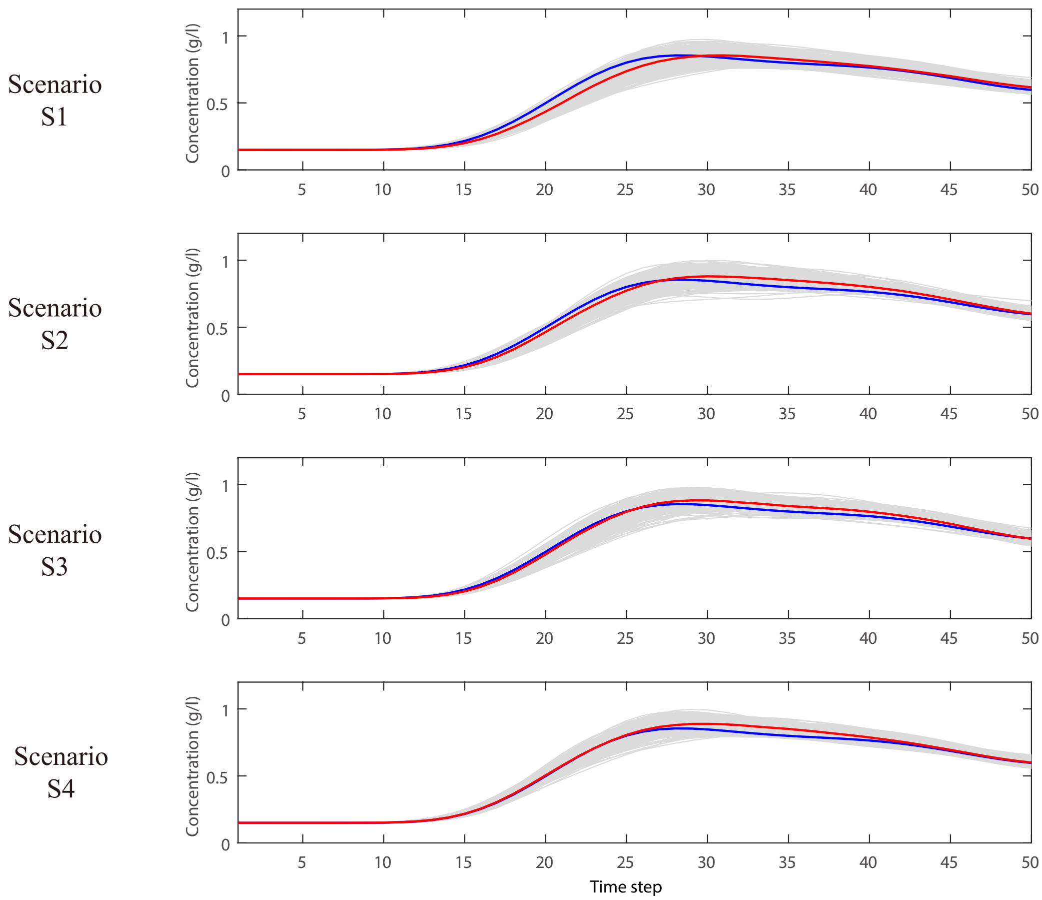

Figure 12: Time evolution of the vertically-averaged concentration of the recovered plume in borehole 3 for all 4 scenarios. The blue curve corresponds to the evolution of the concentration in the reference, while the gray lines are the concentration curves for all 500 realizations, and the red line is the ensemble median.

5. Summary and conclusion

In this paper, we employ the ES-MDA method to identify a contaminant source release curve and hydraulic conductivities by using time-lapse ERT measurements. For this purpose, the study combines a coupled model of groundwater flow, solute transport and geophysics with the ES-MDA assimilation technique. In this data assimilation framework, only the apparent resistivity obtained from the time-lapse ERT measurements is employed to identify the hydraulic conductivities and contaminant release history. The proposed methodology is then validated in a synthetic sandbox with a time-varying release history in a heterogeneous aquifer. The results demonstrate that the CSAC problem could be handled by the proposed approach. The time-varying release history and the main patterns of high conductivity can be captured with proper time-lapse ERT measurements. The plume evolution computed with the updated parameters for both time-varying release curve and spatially-heterogeneous conductivity approximates well the plume computed in the reference field.

Besides, we also analyzed the influence of different AM-BN schemes in our data assimilation framework. Four scenarios with a different number of apparent resistivity measurements (98, 128, 162 and 388) were designed. In scenario S4, the AM-BN scheme with a mixture of three different electrode spacing suffers from data redundancy producing poor results. We believe this is mainly caused by the correlation between the measurements, which is very common in time-lapse ERT surveys and needs to be taken into consideration in further applications.

This study is significant since it is the first time that time-lapse ERT measurements are employed to jointly identify contaminant source information and hydraulic conductivities. But we also admit that a number of issues have not been considered, such as larger ERT measurement errors, different electrode-array configurations, or more complex hydraulic systems. More research is needed in order to move forward and apply this approach to real problems.

6. Acknowledgments

Financial support to carry out this work was received from grants PID2019-109131RB-I00 and PRX17/00150 funded by MCIN/AEI/10.13039/501100011033. Teng Xu also acknowledges the financial support from the Fundamental Research Funds for the Central Universities (B200201015) and Jiangsu Specially-Appointed Professor Program (B19052).

References

Ababou R, Bagtzoglou AC, Mallet A. Anti-diffusion and source identification with the 'RAW' scheme: A particle-based censored random walk. Environmental Fluid Mechanics 2010;10(1):41–76. doi:10.1007/s10652-009-9153-4.

Atmadja J, Bagtzoglou AC. State of the Art Report on Mathematical Methods for Groundwater Pollution Source Identification. Environmental Forensics 2001;2(3):205–14. URL: http://www.sciencedirect.com/science/article/pii/S1527592201900552. doi:http://dx.doi.org/10.1006/enfo.2001.0055.

Ayvaz MT. A linked simulation-optimization model for solving the unknown groundwater pollution source identification problems. Journal of Contaminant Hydrology 2010;117(1-4):46–59. URL: http://dx.doi.org/10.1016/j.jconhyd.2010.06.004. doi:10.1016/j.jconhyd.2010.06.004.

Bagtzoglou AC, Atmadja J. Marching-jury backward beam equation and quasi-reversibility methods for hydrologic inversion: Application to contaminant plume spatial distribution recovery. Water Resources Research 2003;39(2):1–14. doi:10.1029/2001WR001021.

Bagtzoglou AC, Atmadja J. Mathematical Methods for Hydrologic Inversion: The Case of Pollution Source Identification. Water Pollution 2005;5:65–96. URL: http://www.springerlink.com/index/10.1007/b11442. doi:10.1007/b11442.

Bagtzoglou AC, Dougherty DE, Tompson AFB. Application of particle methods to reliable identification of groundwater pollution sources. Water Resources Management 1992;6(1):15–23. doi:10.1007/BF00872184.

Bao J, Li L, Redoloza F. Coupling ensemble smoother and deep learning with generative adversarial networks to deal with non-Gaussianity in flow and transport data assimilation. Journal of Hydrology 2020;590(August):125443. URL: https://doi.org/10.1016/j.jhydrol.2020.125443. doi:10.1016/j.jhydrol.2020.125443.

Bear J. Dynamics of Fluids in Porous Media. American Elsevier, 1972.

Bedekar V, Morway ED, Langevin CD, Tonkin MJ. MT3D-USGS version 1: A US Geological Survey release of MT3DMS updated with new and expanded transport capabilities for use with MODFLOW. Technical Report; US Geological Survey; 2016.

Binley A, Hubbard SS, Huisman JA, Revil A, Robinson DA, Singha K, Slater LD. The emergence of hydrogeophysics for improved understanding of subsurface processes over multiple scales. Water Resources Research 2015;51(6):3837–66. URL: https://doi.org/10.1002/2015WR017016. doi:https://doi.org/10.1002/2015WR017016.

Binley A, Kemna A. DC resistivity and induced polarization methods. In: Hydrogeophysics. Springer; 2005. p. 129–56.

Blanchy G, Saneiyan S, Boyd J, McLachlan P, Binley A. ResIPy, an intuitive open source software for complex geoelectrical inversion/modeling. Computers and Geosciences 2020;137(February):104423. URL: https://doi.org/10.1016/j.cageo.2020.104423. doi:10.1016/j.cageo.2020.104423.

Bouzaglou V, Crestani E, Salandin P, Gloaguen E, Camporese M. Ensemble Kalman filter assimilation of ERT data for numerical modeling of seawater intrusion in a laboratory experiment. Water (Switzerland) 2018;10(4):1–26. doi:10.3390/w10040397.

Butera I, Tanda MG, Zanini A. Simultaneous identification of the pollutant release history and the source location in groundwater by means of a geostatistical approach. Stochastic Environmental Research and Risk Assessment 2013;27(5):1269–80. doi:10.1007/s00477-012-0662-1.

Cao Z, Li L, Chen K. Bridging iterative Ensemble Smoother and multiple-point geostatistics for better flow and transport modeling. Journal of Hydrology 2018;565(August):411–21. URL: https://doi.org/10.1016/j.jhydrol.2018.08.023. doi:10.1016/j.jhydrol.2018.08.023.

Capilla JE, Gömez-Hernández JJ, Sahuquillo A. Stochastic simulation of transmissivity fields conditional to both transmissivity and piezometric head data—3. application to the culebra formation at the waste isolation pilot plan (wipp), new mexico, usa. Journal of Hydrology 1998;207(3-4):254–69.

Capilla JE, Rodrigo J, Gómez-Hernández JJ. Simulation of non-gaussian transmissivity fields honoring piezometric data and integrating soft and secondary information. Mathematical Geology 1999;31(7):907–27.

Carrera J, Neuman SP. Estimation of Aquifer Parameters Under Transient and Steady State Conditions: 1. Maximum Likelihood Method Incorporating Prior Information. Water Resources Research 1986;22(2):199–210. doi:10.1029/WR022i002p00199.

Chen Z, Gómez-Hernández JJ, Xu T, Zanini A. Joint identification of contaminant source and aquifer geometry in a sandbox experiment with the restart ensemble Kalman filter. Journal of Hydrology 2018;564:1074–84. doi:10.1016/j.jhydrol.2018.07.073.

Chen Z, Xu T, Gómez-Hernández JJ, Zanini A. Contaminant Spill in a Sandbox with Non-Gaussian Conductivities: Simultaneous Identification by the Restart Normal-Score

Ensemble Kalman Filter. Mathematical Geosciences 2021;53(7):1587–615. URL: https://doi.org/10.1007/s11004-021-09928-y. doi:10.1007/s11004-021-09928-y.

Cupola F, Tanda MG, Zanini A. Laboratory sandbox validation of pollutant source location methods. Stochastic Environmental Research and Risk Assessment 2015;29(1):169–82. doi:10.1007/s00477-014-0869-4.

Dodangeh A, Rajabi MM, Carrera J, Fahs M. Joint identification of contaminant source characteristics and hydraulic conductivity in a tide-influenced coastal aquifer. Journal of Contaminant Hydrology 2022;247(January):103980. URL: https://doi.org/10.1016/j.jconhyd.2022.103980. doi:10.1016/j.jconhyd.2022.103980.

Emerick AA, Reynolds AC. Ensemble smoother with multiple data assimilation. Computers and Geosciences 2013;55:3–15. URL: http://dx.doi.org/10.1016/j.cageo.2012.03.011. doi:10.1016/j.cageo.2012.03.011.

Evensen G. The Ensemble Kalman Filter: Theoretical formulation and practical implementation. Ocean Dynamics 2003;53(4):343–67. doi:10.1007/s10236-003-0036-9.

Evensen G. Analysis of iterative ensemble smoothers for solving inverse problems. Computational Geosciences 2018;22(3):885–908. URL: http://link.springer.com/10.1007/s10596-018-9731-y. doi:10.1007/s10596-018-9731-y.

Evensen G, Eikrem KS. Conditioning reservoir models on rate data using ensemble smoothers. Computational Geosciences 2018;22(5):1251–70. URL: http://link.springer.com/10.1007/s10596-018-9750-8. doi:10.1007/s10596-018-9750-8.

Feyen L, Gómez-Hernández J, Ribeiro Jr P, Beven KJ, De Smedt F. A bayesian approach to stochastic capture zone delineation incorporating tracer arrival times, conductivity measurements, and hydraulic head observations. Water resources research 2003;39(5).

Franssen H, Gómez-Hernández J. 3d inverse modelling of groundwater flow at a fractured site using a stochastic continuum model with multiple statistical populations. Stochastic Environmental Research and Risk Assessment 2002;16(2):155–74.

Gómez-Hernández J, Franssen HJH, Sahuquillo A. Stochastic conditional inverse modeling of subsurface mass transport: a brief review and the self-calibrating method. Stochastic Environmental Research and Risk Assessment 2003;17(5):319–28.

Gómez-Hernández J, Wen XH. Probabilistic assessment of travel times in groundwater modeling. Stochastic Hydrology and Hydraulics 1994;8(1):19–55.

Gómez-Hernández JJ, Xu T. Contaminant Source Identification in Aquifers: A Critical View. Mathematical Geosciences 2021;:1–22.

Gorelick SM, Evans B, Remson I. Identifying sources of groundwater pollution: An optimization approach. Water Resources Research 1983;19(3):779–90. doi:10.1029/WR019i003p00779.

Harbaugh AW. MODFLOW-2005, the US Geological Survey modular ground-water model: the ground-water flow process. volume 6. US Department of the Interior, US Geological Survey Reston, VA, USA, 2005.

Hendricks Franssen HJ, Kinzelbach W. Real-time groundwater flow modeling with the Ensemble Kalman Filter: Joint estimation of states and parameters and the filter inbreeding problem. Water Resources Research 2008;44(9):1–21. doi:10.1029/2007WR006505.

Jafarpour B, Khodabakhshi M. A Probability Conditioning Method (PCM) for Nonlinear Flow Data Integration into Multipoint Statistical Facies Simulation. Mathematical Geosciences 2011;43(2):133–64. URL: https://doi.org/10.1007/s11004-011-9316-y. doi:10.1007/s11004-011-9316-y.

Jiang X, Ma R, Wang Y, Gu W, Lu W, Na J. Two-stage surrogate model-assisted Bayesian framework for groundwater contaminant source identification. Journal of Hydrology 2021;594(July 2020):125955. URL: https://doi.org/10.1016/j.jhydrol.2021.125955. doi:10.1016/j.jhydrol.2021.125955.

Journel AG, Isaaks EH. Conditional Indicator Simulation: Application to a Saskatchewan uranium deposit. Journal of the International Association for Mathematical Geology 1984;16(7):685–718. doi:10.1007/BF01033030.

Kang X, Shi X, Deng Y, Revil A, Xu H, Wu J. Coupled hydrogeophysical inversion of DNAPL source zone architecture and permeability field in a 3D heterogeneous sandbox by assimilation time-lapse cross-borehole electrical resistivity data via ensemble Kalman filtering. Journal of Hydrology 2018;567:149–64. URL: https://doi.org/10.1016/j.jhydrol.2018.10.019. doi:10.1016/j.jhydrol.2018.10.019.

Kang X, Shi X, Revil A, Cao Z, Li L, Lan T, Wu J. Coupled hydrogeophysical inversion to identify non-Gaussian hydraulic conductivity field by jointly assimilating geochemical and time-lapse geophysical data. Journal of Hydrology 2019;578(August):124092. URL: https://doi.org/10.1016/j.jhydrol.2019.124092. doi:10.1016/j.jhydrol.2019.124092.

Kumar D, Srinivasan S. Ensemble-Based Assimilation of Nonlinearly Related Dynamic Data in Reservoir Models Exhibiting Non-Gaussian Characteristics. Mathematical Geosciences 2019;51(1):75–107. URL: https://doi.org/10.1007/s11004-018-9762-x. doi:10.1007/s11004-018-9762-x.

Kumar D, Srinivasan S. Indicator-based data assimilation with multiple-point statistics for updating an ensemble of models with non-Gaussian parameter distributions. Advances in Water Resources 2020;141:103611. URL: http://www.sciencedirect.com/science/

article/pii/S0309170819309297. doi:https://doi.org/10.1016/j.advwatres.2020.103611.

Le DH, Emerick AA, Reynolds AC. An Adaptive Ensemble Smoother With Multiple Data Assimilation for Assisted History Matching. SPE Journal 2016;21(06):2195–207. URL: https://doi.org/10.2118/173214-PA. doi:10.2118/173214-PA.

Li J, Lu W, Wang H, Fan Y. Identification of groundwater contamination sources using a statistical algorithm based on an improved Kalman filter and simulation optimization. Hydrogeology Journal 2019;27(8):2919–31. URL: http://link.springer.com/10.1007/s10040-019-02030-y. doi:10.1007/s10040-019-02030-y.

Li L, Zhou H, Gómez-Hernández JJ. A comparative study of three-dimensional hydraulic conductivity upscaling at the macro-dispersion experiment (made) site, columbus air force base, mississippi (usa). Journal of Hydrology 2011;404(3-4):278–93.

Li L, Zhou H, Hendricks Franssen HJ, Gómez-Hernández JJ. Groundwater flow inverse modeling in non-MultiGaussian media: Performance assessment of the normal-score Ensemble Kalman Filter. Hydrology and Earth System Sciences 2012;16(2):573–90. doi:10.5194/hess-16-573-2012.

Mao D, Lu L, Revil A, Zuo Y, Hinton J, Ren ZJ. Geophysical Monitoring of Hydrocarbon-Contaminated Soils Remediated with a Bioelectrochemical System. Environmental Science and Technology 2016;50(15):8205–13. doi:10.1021/acs.est.6b00535.

Megdal SB. Invisible water: the importance of good groundwater governance and management. npj Clean Water 2018;1(1):1–5. URL: http://dx.doi.org/10.1038/s41545-018-0015-9. doi:10.1038/s41545-018-0015-9.

Michalak AM, Kitanidis PK. Estimation of historical groundwater contaminant distribution using the adjoint state method applied to geostatistical inverse modeling. Water Resources Research 2004;40(8). doi:10.1029/2004WR003214.

Mirghani BY, Mahinthakumar KG, Tryby ME, Ranjithan RS, Zechman EM. A parallel evolutionary strategy based simulation-optimization approach for solving groundwater source identification problems. Advances in Water Resources 2009;32(9):1373–85. URL: http://dx.doi.org/10.1016/j.advwatres.2009.06.001. doi:10.1016/j.advwatres.2009.06.001.

Neupauer RM, Wilson JL. Adjoint method for obtaining backward-in-time location and travel time probabilities of a conservative groundwater contaminant. Water Resources Research 1999;35(11):3389–98. doi:10.1029/1999WR900190.

Panjehfouladgaran A, Rajabi MM. Contaminant source characterization in a coastal aquifer influenced by tidal forces and density-driven flow. Journal of Hydrology 2022;610(April):127807. URL: https://doi.org/10.1016/j.jhydrol.2022.127807. doi:10.1016/j.jhydrol.2022.127807.

Pirot G, Krityakierne T, Ginsbourger D, Renard P. Contaminant source localization via Bayesian global optimization. Hydrology and Earth System Sciences 2019;23(1):351–69. doi:10.5194/hess-23-351-2019.

Power C, Gerhard JI, Tsourlos P, Giannopoulos A. A new coupled model for simulating the mapping of dense nonaqueous phase liquids using electrical resistivity tomography. Geophysics 2013;78(4). doi:10.1190/GEO2012-0395.1.

Rafiee J, Reynolds AC. Theoretical and efficient practical procedures for the generation of inflation factors for ES-MDA. Inverse Problems 2017;33(11). doi:10.1088/1361-6420/aa8cb2.

Revil A, Qi Y, Ghorbani A, Soueid Ahmed A, Ricci T, Labazuy P. Electrical conductivity and induced polarization investigations at Krafla volcano, Iceland. Journal of Volcanology and Geothermal Research 2018;368:73–90. doi:10.1016/j.jvolgeores.2018.11.008.

Seferou P, Soupios P, Kourgialas NN, Dokou Z, Karatzas GP, Candasayar E, Papadopoulos N, Dimitriou V, Sarris A, Sauter M. Olive-oil mill wastewater transport under unsaturated and saturated laboratory conditions using the geoelectrical resistivity tomography method and the FEFLOW model. Hydrogeology Journal 2013;21(6):1219–34. doi:10.1007/s10040-013-0996-x.

Sen PN. Influence of temperature on electrical conductivity on shaly sands 1992;57(1):89–96.

Shao S, Guo X, Gao C, Liu H. Quantitative relationship between the resistivity distribution of the by-product plume and the hydrocarbon degradation in an aged hydrocarbon contaminated site. Journal of Hydrology 2021;596(February):126122. URL: https://doi.org/10.1016/j.jhydrol.2021.126122. doi:10.1016/j.jhydrol.2021.126122.

Skaggs TH, Kabala ZJ. Recovering the release history of a groundwater contaminant. Water Resources Research 1994;30(1):71–9. URL: http://doi.wiley.com/10.1029/93WR02656. doi:10.1029/93WR02656.

Sun AY, Painter SL, Wittmeyer GW. A constrained robust least squares approach for contaminant release history identification. Water Resources Research 2006;42(4):1–13. doi:10.1029/2005WR004312.

Todaro V, D'Oria M, Tanda MG, Gómez-Hernández JJ. Ensemble smoother with multiple data assimilation to simultaneously estimate the source location and the release history of a contaminant spill in an aquifer. Journal of Hydrology 2021;598(April). doi:10.1016/j.jhydrol.2021.126215.

Tso ChM, Johnson TC, Song X, Chen X, Kuras O, Wilkinson P, Uhlemann S, Chambers J, Binley A, Centre LE. Integrated hydrogeophysical modelling and data assimilation for geoelectrical leak detection. Journal of Contaminant Hydrology 2020;234(July):103679. URL: /doi.org/10.1016/j.jconhyd.2020.103679. doi:10.1016/j.jconhyd.2020.103679.

Wen XH, Capilla JE, Deutsch C, Gómez-Hernández J, Cullick A. A program to create permeability fields that honor single-phase flow rate and pressure data. Computers & Geosciences 1999;25(3):217–30.

Woodbury AD, Ulrych TJ. Minimum relative entropy inversion: Theory and application to recovering the release history of a groundwater contaminant. Water Resources Research 1996;32(9):2671–81.

Xia T, Dong Y, Mao D, Meng J. Delineation of LNAPL contaminant plumes at a former perfumery plant using electrical resistivity tomography. Hydrogeology Journal 2021;8(1):1189–201.

Xu T, Gómez-Hernández JJ. Joint identification of contaminant source location, initial release time, and initial solute concentration in an aquifer via ensemble Kalman filtering. Water Resources Research 2016;doi:10.1002/2014WR016618.Received.

Xu T, Gómez-Hernández JJ, Chen Z, Lu C. A comparison between ES-MDA and restart EnKF for the purpose of the simultaneous identification of a contaminant source and hydraulic conductivity. Journal of Hydrology 2021;595:125681. URL: https://www.sciencedirect.com/science/article/pii/S0022169420311422. doi:https://doi.org/10.1016/j.jhydrol.2020.125681.

Xu T, Jaime JG. Simultaneous identification of a contaminant source and hydraulic conductivity via the restart normal-score ensemble Kalman filter. Advances in Water Resources

2018;112(July 2017):106–23. URL: https://doi.org/10.1016/j.advwatres.2017.12.011. doi:10.1016/j.advwatres.2017.12.011.

Xu T, Zhang W, Gómez-Hernández JJ, Xie Y, Yang J, Chen Z, Lu C. Non-point contaminant source identification in an aquifer using the ensemble smoother with multiple data assimilation. Journal of Hydrology 2022;606(January):127405. doi:10.1016/j.jhydrol.2021.127405.

Zeng L, Shi L, Zhang D, Wu L. A sparse grid based Bayesian method for contaminant source identification. Advances in Water Resources 2012;37:1–9. URL: http://dx.doi.org/10.1016/j.advwatres.2011.09.011. doi:10.1016/j.advwatres.2011.09.011.

Zheng C, Wang PP. MT3DMS: A Modular Three-Dimensional Multispecies Transport Model 1999;(December):219.

Zhou B, Greenhalgh SA. Cross-hole resistivity tomography using different electrode configurations. Geophysical Prospecting 2000;48(5):887–912. doi:10.1046/j.1365-2478.2000.00220.x.

Zhou H, Gómez-Hernández JJ, Hendricks Franssen HJ, Li L. An approach to handling non-Gaussianity of parameters and state variables in ensemble Kalman filtering. Advances in Water Resources 2011;34(7):844–64. URL: http://dx.doi.org/10.1016/j.advwatres.2011.04.014. doi:10.1016/j.advwatres.2011.04.014.

Zhou H, Gómez-Hernández JJ, Li L. Inverse methods in hydrogeology: Evolution and recent trends. Advances in Water Resources 2014;63:22–37. URL: http://dx.doi.org/10.1016/j.advwatres.2013.10.014. doi:10.1016/j.advwatres.2013.10.014.